

Signatures of metal to insulator crossover in the repulsive Fermi Hubbard model through static correlations

Sayantana Roy,¹ Sameed Pervaiz,¹ Thereza Paiva,² and Nandini Trivedi¹

¹*Department of Physics, The Ohio State University, Columbus OH 43210, USA*

²*Instituto de Física, Universidade Federal do Rio de Janeiro Cx.P. 68.528, 21941-972 Rio de Janeiro RJ, Brazil*

(Dated: March 22, 2024)

Cold atom systems provide a rich platform to realize strongly interacting condensed matter systems, and recent progress in fluorescence imaging technique has enabled identification of nontrivial doublon, singlon, and holon correlation functions. We show that these correlators can be used to identify the conditions under which local moments form in an interacting electronic system. Toward this end, we report a Determinantal Quantum Monte Carlo (DQMC) study of such correlation functions in the two-dimensional repulsive Fermi Hubbard model on a square lattice as a function of doping, interaction strength and temperature. We find definite signatures of the crossover from small U (band regime) to large U (correlated insulator regime). Our key findings are: (1) An opening of a charge gap in the thermodynamic density of states is accompanied by the appearance of temperature insensitive points in the equation of state at finite doping, which can be used to distinguish the band regime in cold atom experiments. (2) Nearest neighbor doublon holon correlations track the opening of charge gap; these compete with density correlations to generate moment moment correlations that show different behavior in the metallic and correlated insulator regime. (3) Non local correlation functions can be used to distinguish between the two regimes, both at and away from half filling. Our results allow comparisons of different correlation functions with recent experimental findings and guide further experimental investigations.

I. INTRODUCTION

The repulsive Fermi-Hubbard model is a simple yet apt prototype for understanding the behavior of strongly-correlated many-body systems, proposed independently by Gutzwiller[1], Kanamori[2] and Hubbard[3], and thought to be a model for explaining high T_C superconductivity by Anderson[4]. Despite the introduction of the Hubbard model around 60 years ago, the solution of the problem is not known analytically in $d > 1$. As such, numerical and experimental efforts remain viable candidates to study it. Given the complexity of many-body interactions, controversies about the phase diagram and lattice geometry dependence of the phases remain despite significant progress[5]. Experiments involving fermions confined to two-dimensional lattices have led to measurements of a wealth of quantum mechanical and thermodynamic quantities in agreement with predictions such as the appearance of both metallic and Mott insulating phases within such quantum gases [6–17].

Of particular interest is the metal-insulator transition in strongly correlated system, where a Fermi liquid with finite kinetic energy and small temperature-dependent entropy approaches a $\log 2$ entropy paramagnetic insulator. At the critical point, the Fermi liquid effective mass diverges to match the entropy of the insulating state[18]. In the Hubbard model, this scenario is complicated by the presence of an antiferromagnetic state, which might make the Mott transition hidden or apparent dependent on lattice constraints and frustration [19]. The metal-insulator transition is a first-order transition, with co-existing metallic and insulator phases in a small region in the $U - T$ plane, before it gives away to a crossover between metal and paramagnetic insulator with short-

range correlations at higher temperatures[20]. Experimental evidence of metal-insulator transitions has been studied by a variety of techniques such as transport measurements [21], susceptibility measurements[22], ARPES measurements [23], STM [24], to name a few.

Cold atomic systems provide the advantage of creating specific hamiltonians[25–31]; where measurements of physical quantities can be compared directly with theoretical modeling[32–34]. Early quantum gas microscope experiments were very successful in measuring spin-spin correlation functions ([8, 16, 35]). Not only were they able to measure near-neighbour correlation functions (in excellent agreement with QMC and NLCE data), but longer ranged measurements that probed spin-spin correlation functions [16]. Developments in quantum gas microscope technology have furthermore allowed experimentalists to produce not only site-resolved measurements of local moment, [8], but that of the local number, doublon, and holon densities [36], as well as correlation functions between these quantities[7, 8, 10, 13, 17, 28, 37–54]. Correlation functions at distances beyond nearest-neighbor display a nontrivial dependence on interactions and doping, studying them may lead to a new understanding of the physics at play. A new development was the construction of a bilayer Fermi gas microscope [36, 37], in which each lattice site is split into a double well, separating atom pairs. This allows for measurement of all possible correlation functions between doubly occupied, singly occupied, and empty sites. In light of these recent advances, it is natural to ask (a) Given that the metal-insulator crossover has been observed through density fluctuations[9], are there additional correlation functions that can track it in quantum gas experiments at intermediate temperatures? (b) What are the distinct

measurements for thermodynamic variables and correlation functions to probe such a crossover behavior, if they do show significantly different behavior between the metallic and insulating regimes?

We seek to answer these questions in this work; in the intermediate temperature range, Determinant Quantum Monte Carlo [55–57] is not plagued by the infamous “sign” problem and is a powerful tool to perform unbiased numerical simulations. In this context, we have investigated both thermodynamic observables (equation of state, compressibility, thermodynamic entropy and doublon number) as well as equal time correlation functions (between density, doublons, holons and local moments) in the square lattice single band repulsive Hubbard model as functions of doping, temperature and interaction strength. Our key findings are as follows:

(1) Temperature dependence of thermodynamic density of states $\frac{\partial n}{\partial \mu}$, evaluated at half filling, shows values of U/t , at which a charge gap opens in the thermodynamic density of states. This is accompanied by the appearance of “isosbestic” points (special μ values) at finite doping in the equation of state $n(\mu)$ where the temperature variation vanishes. Temperature dependence of average doublon number also indicates an “insulating” and “metallic” regime (explained in Sec III), which may not be concurrent with the crossover observed through the charge gap opening, indicating a second “magnetic” crossover scale.

(2) Doublon-holon correlations between neighboring sites, evaluated at half filling show distinct behavior across the “charge” crossover and “magnetic” crossover scales. The development of singlet pairs between nearest neighbor sites can be viewed as a competition between nearest neighbor “attractive” doublon-holon pairs and “repulsive” density-density pairs. Moment moment correlations are maximal at intermediate U/t , although individual moments get formed better with increasing U/t .

(3) The crossover from metallic regime (band-like description) to correlated insulator regime (local moment-like description) has effects on the structure of non-local correlation functions beyond the nearest neighbors, both at and away from half filling. Tracking these correlations with increasing U/t can also be used to probe the crossover between the metallic and correlated insulator regimes, at the appropriate doping and temperature.

The rest of the paper is organized as follows: In section II, we introduce the model and discuss the parameter ranges explored in our simulations. In section III, we review the notion of charge gap, and how compressibility and doublon occupancy can capture interplay of interaction and doping dependent physics. In section IV, we introduce equal time correlation functions that can be measured in cold atom experiments, and show their doping dependence at different temperature and interaction strength; in particular, we show how these correlators can capture the metallic regime to correlated insulator regime crossover. In section V, we show how non local

correlators can distinguish between metallic and correlated insulator regime, at and away from half filling. In section VI, we compare our numerical results with equal time correlators measured by a bilayer quantum gas microscope with ultracold atoms [36]. Finally, we conclude with a brief overview of our results and the possibility of observing small U to large U crossover in the repulsive Fermi Hubbard model experimentally with cold atomic systems.

II. MODEL AND METHOD

We consider the single band Fermi Hubbard model with nearest neighbor hopping and onsite repulsive interaction, defined by the hamiltonian,

$$\mathcal{H} = -t \sum_{\langle i,j \rangle, \sigma} \left(\hat{c}_{i,\sigma}^\dagger \hat{c}_{j,\sigma} + h.c. \right) - \mu \sum_i \hat{n}_i + U \sum_i \left(\hat{n}_{i\uparrow} - \frac{1}{2} \right) \left(\hat{n}_{i\downarrow} - \frac{1}{2} \right) \quad (1)$$

We write the Hamiltonian in a particle-hole symmetric form so that when the chemical potential $\mu = 0$, the system is half filled. Here t is the tunneling amplitude for a fermion to hop from one site to the nearest neighbor and U is the strength of the on-site repulsion. The spatial index i labels a site on a 2D square lattice, and $\hat{c}_{i,\sigma}$ and $\hat{c}_{i,\sigma}^\dagger$ are fermionic annihilation and creation operators respectively. The number operator is defined as $\hat{n}_{i,\sigma} \equiv \hat{c}_{i,\sigma}^\dagger \hat{c}_{i,\sigma}$, $\hat{n}_i = \hat{n}_{i,\uparrow} + \hat{n}_{i,\downarrow}$, and the particle density per site $n = \sum_i \langle \hat{n}_i \rangle / N_s$, where N_s is the total number of sites.

We perform Determinant Quantum Monte Carlo (DQMC) simulations that maps a many-particle interacting fermionic system into a single-particle Hamiltonian (quadratic form), with the aid of bosonic auxiliary fields. For the analyses conducted in this paper, ensembles of 10x10 lattices are simulated over a finite set of chemical potentials and different interaction strengths from weak to strong coupling. We look at evolution of the equation of state (n vs μ), thermodynamic density of states $\tilde{\kappa} = \kappa n^2 = \frac{\partial n}{\partial \mu}$, doublon occupancy $d = \langle n_\uparrow n_\downarrow \rangle$ and thermodynamic entropy s across the metal-insulator crossover in the square lattice, with increasing U/t . We also look at the interplay between various charge degrees of freedom, from the weak coupling to the strong coupling limit, by investigating equal time correlation functions between holons, doublons, and local moments.

For sufficiently low temperatures, moderate-range antiferromagnetic correlations are expected to be maximal at $U/t \approx 8$ [8], when the interaction energy equals the single particle bandwidth. Simulations are performed at temperatures $T/t \in [0.33, 2.0]$, with $\mu \in [-10.0, 10.0]$ to study evolution of correlation functions across the metal-insulator crossover. We have restricted our analysis to parameter regimes where the sign problem is not an issue,

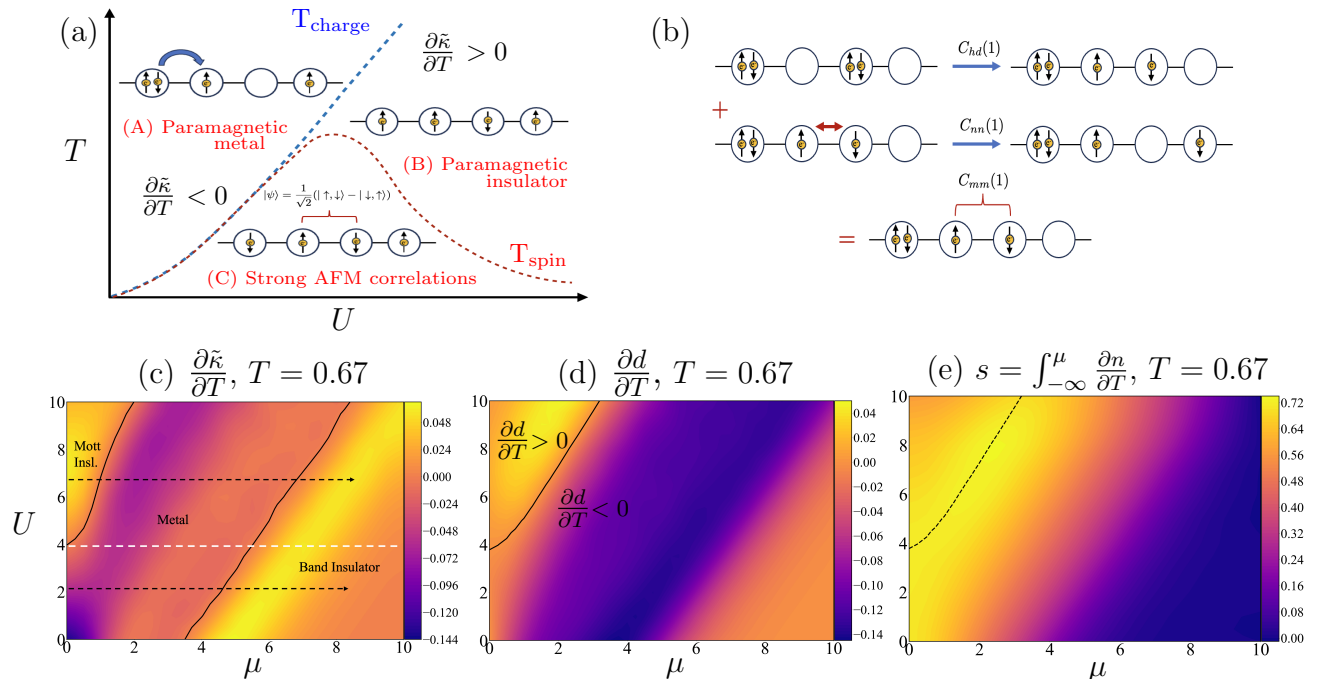


FIG. 1: (a) Temperature and interaction scales in the 2D square lattice Hubbard model at half filling. There are two energy scales, the charge gap Δ_{ch} , which sets the energy scale for charge fluctuations, and spin gap Δ_S , which sets energy scales for spin fluctuations. The corresponding temperature scales separate the $U - T$ plane at half filling into three regions: (A) Metallic – for $T > T_{\text{charge}}(U)$, the system is a paramagnetic metal. (B),(C) Mott Insulator with single fermion per site. (B) Correlated Insulator – below the temperature scale $T_{\text{charge}}(U)$, the system is a paramagnetic insulator, driven by strong onsite repulsion. Itinerant fermions get pinned down to form local moments, however, the moments are not yet correlated due to thermal fluctuations. (C) Short range ordered state with strong AF correlations – on lowering the temperature below $T_{\text{spin}}(U)$, the Mott-insulator develops strong antiferromagnetic correlations that are short ranged. (b)-(e) Main ideas explored in this work. (b) Moment development between neighboring sites $C_{mm}(1)$ can be viewed as a competition between “attractive” doublon-holon pairs $C_{hd}(1)$ that can fluctuate to form singlets, and “repulsive” density density pairs $C_{nn}(1)$ that push them away. Due to this competition, moment correlations show nontrivial doping and interaction strength dependence (discussed in Sec IV C). (c) Temperature variation of the thermodynamic density of states, $\tilde{\kappa} = \frac{\partial n}{\partial \mu} = \kappa n^2$ which serves as proxy for charge gap, separates the $U - \mu$ plane at fixed temperature into (I) Mott insulator, (II) Metallic and (III) Band Insulator phase (Fig 2(d)-(e)). The system is “gapless” (metallic regime) below the white dashed line for all dopings, and “gapped” (insulating regime) above due to the presence of a correlation driven insulating phase near half-filling. Correlation functions between doublon, holon, local moments and density pairs are studied across these three regimes, shown schematically by the black arrows. (d) Temperature variation of average double occupancy d also divides the $U - \mu$ plane into an insulator-like region where local moment formation increases as the system is cooled, $\frac{\partial d}{\partial T} > 0$, and a metallic region where double occupancy increases as the system is cooled, $\frac{\partial d}{\partial T} < 0$. This can be used in conjunction with $\frac{\partial \tilde{\kappa}}{\partial T}$ to identify doping-dependent phases at the appropriate T and U (Fig 2(g)) (e) Thermodynamic entropy, $s(U, \mu, T)$ in the $U - \mu$ plane. The black dashed line denotes the contour along which $\frac{\partial d}{\partial T} = 0$ in panel (d). Note that this approximately follows the maxima of the entropy. (All energy scales in the figures are in units of t).

and at temperatures for which the coherence length is smaller than the system size. For comparison with recent experimental data, that features an interaction strength of $U/t = 11.8$ and a temperature of $T/t = 0.69$ [36], we present data for $U/t = 11.8$ and $T/t = 1.25, 1.43, 1.6$. For local/nonlocal correlators of the density, local moment, doublons and holons, calculations were performed over 20 simulations at each (U, μ, T) , with 2000 warmup sweeps and 5000 measurement sweeps; measurement errors remain small enough to make meaningful observations. For calculating derivatives, a grid of $\delta\mu = 0.5$ and $\delta\beta = 0.1$ was employed.

III. MOTTNESS AND CHARGE GAP

The onset of “Mottness” is characterized by the formation of a charge gap, which is exponentially small in the weak coupling limit: $\Delta_c \propto e^{-2\pi\sqrt{\frac{t}{U}}}$, but becomes proportional to the interaction strength in the strong coupling limit: $\Delta_c \propto U$. The onset of “Mottness” is shown in Fig 2, where the n vs μ curves start to flatten around half-filling at $U/t = 4$, and the Mott plateau is prominent at $U/t = 8.0$ for the temperature range studied.

A distinct signature of the formation of Mott plateau is

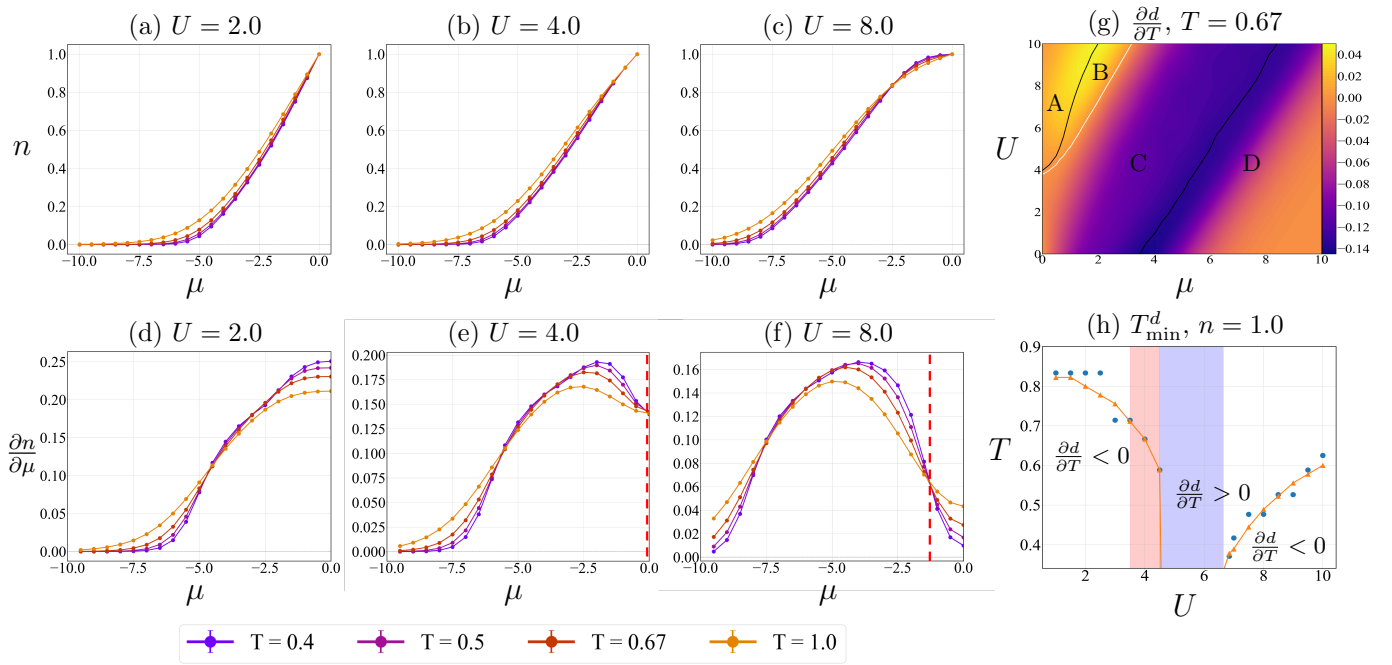


FIG. 2: (a)-(c) Equation of state $n(\mu)$ of the 2D Hubbard model on square lattice with varying U/t . (a) $U/t = 2.0$, (b) $U/t = 4.0$, (c) $U/t = 8.0$. Note that beyond $U/t = 4.0$, there are special values for μ close to half filling, where n vs μ show narrow crossings for the different values of T/t examined, in conjunction with the development of a Mott plateau. (d)-(e) Thermodynamic density of states $\tilde{\kappa} = \frac{\partial n}{\partial \mu} = \kappa n^2$ (where κ is the compressibility), as a function of U/t . (d) $U/t = 2.0$, (e) $U/t = 4.0$, (f) $U/t = 8.0$. The “special” μ points close to half filling, where $\tilde{\kappa}$ becomes insensitive to temperature (marked by vertical red dashed lines), approximately track the edges of the many body bands; this signifies opening of a charge gap, at these μ points. (g)-(h) Average doublon number at finite temperatures. (g) Temperature variation of $d = \langle n_{i\uparrow} n_{i\downarrow} \rangle$ and $\tilde{\kappa}$ at $T/t = 0.67$ divides the $U - \mu$ plane into 4 distinct regions; black lines mark contour of zeros of $\frac{\partial \tilde{\kappa}}{\partial T}$ in the $U - \mu$ plane, and white lines mark zeros of $\frac{\partial d}{\partial T}$. (A) Correlated insulator, both $\frac{\partial \tilde{\kappa}}{\partial T}$ and $\frac{\partial d}{\partial T} > 0$; (B) Anomalous metal, $\frac{\partial \tilde{\kappa}}{\partial T} < 0$, $\frac{\partial d}{\partial T} > 0$; (C) Metal, $\frac{\partial \tilde{\kappa}}{\partial T} < 0$, $\frac{\partial d}{\partial T} < 0$; (D) Band Insulator, $\frac{\partial \tilde{\kappa}}{\partial T} > 0$, $\frac{\partial d}{\partial T} < 0$. (h) Temperature at which d exhibits a minima, T_{\min}^d , at half filling. Blue dots denote temperatures obtained directly from QMC data, orange triangles denote temperature obtained by fitting $d(T)$ with a polynomial function. Red shaded region denotes metal-insulator crossover window in the range $T/t \in [0.33, 1.0]$, as determined by $\frac{\partial \tilde{\kappa}}{\partial T}$ (Fig 3). In the weak coupling regime, the initial decrease in d is to access the larger spin entropy of paramagnet, $S \propto \ln 2$, with T_{\min}^d coinciding with quasiparticle coherence temperature, $T_F^*(U)$ [58]. For $U/t \in (4.5, 6.7)$, (blue shaded region) no minima in $d(T)$ was found upto lowest temperature considered here, $T/t = 0.33$. (All energy scales in the figures are in units of t).

the appearance of “isosbestic points”, where the density curves for different temperatures cross at a narrow range of chemical potentials, close to half filling point $\mu = 0.0$. This temperature independence is not seen in the weak coupling limit, where our data is above the exponentially small charge gap. The thermodynamic density of states $\tilde{\kappa}$ presents a similar feature. Around the finite values of chemical potential where $\tilde{\kappa}$ becomes insensitive to temperature, the system goes from being more compressible with decreasing temperature (metallic), to less compressible with decreasing temperature (insulating). This signifies the opening of a Mott gap, at a critical $U_c(T)$. The location of these “isosbestic” points are crucial to the sign change in the Seebeck coefficient calculated from thermodynamic quantities, as seen in Ref [59, 60].

An alternate way to study effects of correlation is to look at the average doublon occupancy, $d = \langle n_{i\uparrow} n_{i\downarrow} \rangle$. Coupled with $\tilde{\kappa}$, average doublon occupation can cap-

ture interplay between interaction and doping dependent physics, as shown in Fig 2 (g)-(h). Previous Diagrammatic QMC studies have pointed out existence of a Non-Fermi Liquid like region in the $T - U$ phase diagram at half filling, based on separation of temperature scales at which $\frac{\partial n}{\partial \mu}$ and potential energy or $\varepsilon^{\text{pot}} = Ud$ change variation with temperature[61]. In a metal, $\frac{\partial d}{\partial T} < 0$, signalling that electrons are itinerant and can form double occupancies on cooling. However, in a correlation driven insulator, $\frac{\partial d}{\partial T} > 0$ due to effects of onsite repulsion, which leads to localization by formation of local moments on cooling[58, 61, 62]. This behavior, in conjunction with $\frac{\partial \tilde{\kappa}}{\partial T}$, divides the $U - \mu$ plane at a finite temperature into distinct regions, shown in Fig 2(g). The black line marks the zeros of $\frac{\partial \tilde{\kappa}}{\partial T}$, the white line marks the zeros of $\frac{\partial d}{\partial T}$. In Region (A) the system is Mott insulating, as both $\frac{\partial \tilde{\kappa}}{\partial T}$ and $\frac{\partial d}{\partial T}$ are positive. In Region (C) the system is metal-

lic, as both $\frac{\partial d}{\partial T}$ and $\frac{\partial \bar{n}}{\partial T}$ are negative. However, there exists a doping-dependent anomalous metallic region (B), where compressibility dictates that the system is metallic ($\frac{\partial \bar{n}}{\partial T} < 0$), but doublon number dictates that it should be insulating through the formation of moments as the system is cooled ($\frac{\partial d}{\partial T} > 0$). This implies the existence of a compressible system at intermediate temperature range where a Fermi liquid description might not be valid. Note that the transition from a correlated insulator to metallic behavior happens along the line of maximum of $\frac{\partial d}{\partial T}$, whereas the transition from a metal to band insulator happens along the line of minimum of $\frac{\partial d}{\partial T}$. The zeros of $\frac{\partial d}{\partial T}$ approximately follows the peak of thermodynamic entropy in Fig 1(e). This is expected as the number of possible configurations for the ground state is maximized; the system has a tendency to form both local moments and doublons on cooling.

The schematic phase diagram shown in Fig 2(g) can be complicated at lower temperatures, due to the nature of $d(T)$ at half filling, shown in Fig 2(h). Polynomial fits provide temperatures where the doublon number reaches its minima, T_{min}^d . This further divides the $T - U$ plane at half filling into 3 regions based on sign of $\frac{\partial d}{\partial T}$; in the metallic phase (left of the red shaded region), quasiparticle coherence persists upto finite temperature[58], and coherence temperature decreases with U/t . On crossover into the insulating phase, as dictated by the charge gap (right of the red shaded region), this behavior is quickly lost, and average doublon number monotonically decreases with cooling upto lowest temperature considered here ($T = 0.33t$), signifying increased localization of electrons. On increasing U/t further into the Mott insulating side, average doublon number develops a minima at a finite temperature, in stark contrast to DMFT studies in 3D [58]; such behavior was also observed in [19, 63]. This defines a fan shaped region in the $U - T$ plane, where $\frac{\partial d}{\partial T}$ is always positive.

The range of U/t , which we dub the ‘‘magnetic’’ crossover window (in which local moment formations are favored down to lowest temperatures studied here) is different from the U/t window in the range of temperatures considered here, in which charge gap dictates a metal insulator crossover (blue shaded region vs red shaded region in Fig 2(h)), with the possibility that the two might coincide at lower temperatures $T/t < 0.33$. However, these two can be used in conjunction to define a larger crossover window in both the charge density and local moment channels. As we will show in later section, nearest neighbor moment moment correlation function at half filling also peak inside this range of interaction for which no minima was found in $d(T)$.

IV. EQUAL TIME CORRELATION FUNCTIONS

To study the evolution of the correlation functions between the metallic and correlated insulator regime, we define local degrees of freedom - double occupations, holons

and singlons as:

$$\begin{aligned} d_i &= n_{i\uparrow}n_{i\downarrow} \\ h_i &= (1 - n_{i\uparrow})(1 - n_{i\downarrow}) = 1 - n_i + d_i \\ s_i &= (n_{i\uparrow} - n_{i\downarrow})^2 = n_i - 2d_i = 1 - d_i - h_i \end{aligned} \quad (2)$$

Note that the definition of singlons is identical to the definition of local moments, given by [64]

$$\begin{aligned} \langle m^2 \rangle &= C(\mathbf{r}=\mathbf{0}), \\ C(\mathbf{r}) &= \sum_{\mathbf{i}} \langle (n_{\mathbf{i}+\mathbf{r},\uparrow} - n_{\mathbf{i}+\mathbf{r},\downarrow})(n_{\mathbf{i},\uparrow} - n_{\mathbf{i},\downarrow}) \rangle \end{aligned} \quad (3)$$

Local moments help in understanding the development of magnetic correlations as a function of U . At $U/t \rightarrow \infty$, double occupations and holes at half-filling are completely eliminated, and $m^2 \rightarrow 1$. In the strong coupling limit, local moments start to form at a temperature scale $T_{ch} \propto U$, the charge gap, and short range antiferromagnetic correlations (in 2D) develop below the spin gap temperature scale, $T_{spin} \propto \frac{t^2}{U}$. In contrast, in the weak coupling limit, antiferromagnetic correlations develop due to instability of the Fermi surface by perfect nesting through $\mathbf{Q} = (\pi, \pi)$ wave vector at half filling; this leads to an increased susceptibility due to spin density wave formation that doubles the unit cell and gaps out the excitation spectra, $\Delta \propto e^{-2\pi\sqrt{t/U}}$. This crossover from a spin density wave (Slater) insulator to a Mott(Heisenberg) insulator in the repulsive Hubbard model is the analog of the BCS-BEC crossover in the attractive Hubbard model [63].

Equal time correlation functions can track the weak coupling to strong coupling evolution of the Hubbard model. Density density correlations keep track of the number fluctuation and hence formation of the Mott gap[9, 65–67]. In the strong coupling regime, doublon-holon fluctuations contribute to generating singlet pairs between neighboring sites [68]. In this section, we look at interplay between density density and holon doublon pairs, and show how development of nearest neighbor moment moment correlation can arise due to competition between them. We study nonlocal correlation functions between nearest neighbor sites belonging to different sublattices, C^{A-B} , as a function of doping for various interaction strengths, at a fixed temperature of $T/t = 0.5$.

A. Density density correlation functions

The central quantity to probe for opening of a charge gap is the connected density-density correlation function, which captures the number density fluctuations [9]. It is defined by:

$$C_{nn}(r) = \frac{1}{N_s} \sum_{\mathbf{i}} \langle n_{\mathbf{i}+\mathbf{r}}n_{\mathbf{j}\mathbf{i}} \rangle - \langle n_{\mathbf{i}+\mathbf{r}} \rangle \langle n_{\mathbf{i}} \rangle \quad (4)$$

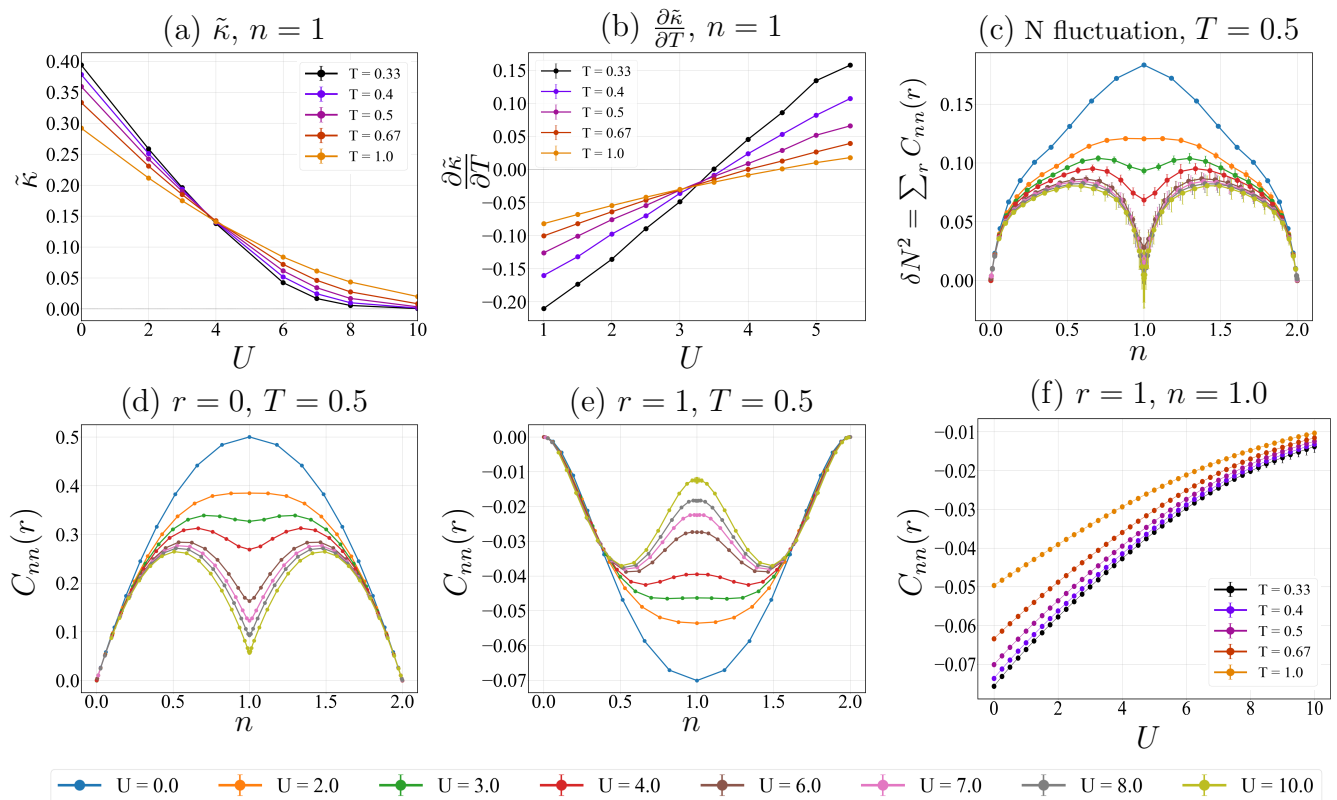


FIG. 3: (a)-(b)- Thermodynamic density of states for the 2D Hubbard model on square lattice. (a) $\tilde{\kappa} = \frac{\partial n}{\partial \mu}$ at half filling. Note that for $U/t \in (3.5, 4.5)$, $\tilde{\kappa}$ becomes insensitive to temperature (in the range we study here) at various $U_c(T)/t$. This denotes a crossover window $U/t \in (3.5, 4.5)$ from a metallic regime (in which $\tilde{\kappa}$ grows with decreasing temperature) to a correlated insulator regime (in which $\tilde{\kappa}$ decreases with decreasing temperature). Crossover points correspond to values of U/t for which the equation of state shows the opening of a charge gap in Fig 2(d)-(e). (b) Location of the crossover point $U_c(T)$, at half filling, calculated from $\frac{\partial \tilde{\kappa}}{\partial T} = 0$ at various T . (c) Number density fluctuations calculated by summing density correlation function over all possible pairs also captures this behavior and shows the formation of a dip for $U/t \geq 3.0$, shown for $T/t = 0.5$ as a function of doping. (d)-(e) Contributions of density fluctuations to the compressibility. (d) Onsite fluctuations $C_{nn}(r = 0)$ that are always positive; (e) Nearest neighbor fluctuations $C_{nn}(r = 1)$ that are always negative. Both (d) and (e) show formation of a dip in magnitude at half filling, at $U/t \geq 3.0$, which signifies opening of Mott gap. (f) Next nearest neighbor density correlations at half filling; density correlations decrease monotonically in magnitude at all temperatures, with increasing U/t , due to onsite repulsion. (All energy scales in the figures are in units of t).

where N_s is the number of lattice sites. We can extract the compressibility from the fluctuation-dissipation theorem

$$\kappa n^2 = \frac{\partial n}{\partial \mu} = \beta \sum_{\mathbf{r}} \langle n_{\mathbf{i}+\mathbf{r}} n_{\mathbf{i}} \rangle_C \quad (5)$$

It is a nontrivial check of our numerics that the total number fluctuation given by RHS of Eq. 5 and $\partial n / \partial \mu$ agree. In the metallic regime, the chemical potential μ lies inside the band; increasing temperature causes particles to occupy higher energy states, thus decreasing number of occupied states at μ , so $\frac{\partial n}{\partial \mu}$ should decrease with temperature. In the correlated insulator regime, μ lies in the gap and the density fluctuations should be thermally activated; $\frac{\partial n}{\partial \mu}$ should increase with temperature. The behavior of the compressibility as a function of U/t is shown

in Fig 3 (a), which clearly shows the crossover at half filling from metallic to correlated insulator behavior. The vanishing of the temperature dependence $\tilde{\kappa}$, shown for a few temperatures in Fig 3(b), sets the interaction energy scale, $U/t \in (3.5, 4.5)$ for crossover from the metallic to the insulating behavior in the temperature ranges considered here. Earlier studies with Diagrammatic QMC at lower temperatures had found this to occur around $U \in (2, 3.5)$ [61]; increasing the temperature pushes the crossover points to higher U/t , as long as the temperature is below the charge gap.

Fig 3 (c) shows the total density fluctuations for $T/t = 0.5$, obtained by Eq.5. At half filling, a dip in the density fluctuation develops after $U/t \sim 3.0$, which follows from a dip in the local and nearest neighbor density-density correlation function (shown in Fig 3(d), (e)), which are the most dominant contributions to the density fluctua-

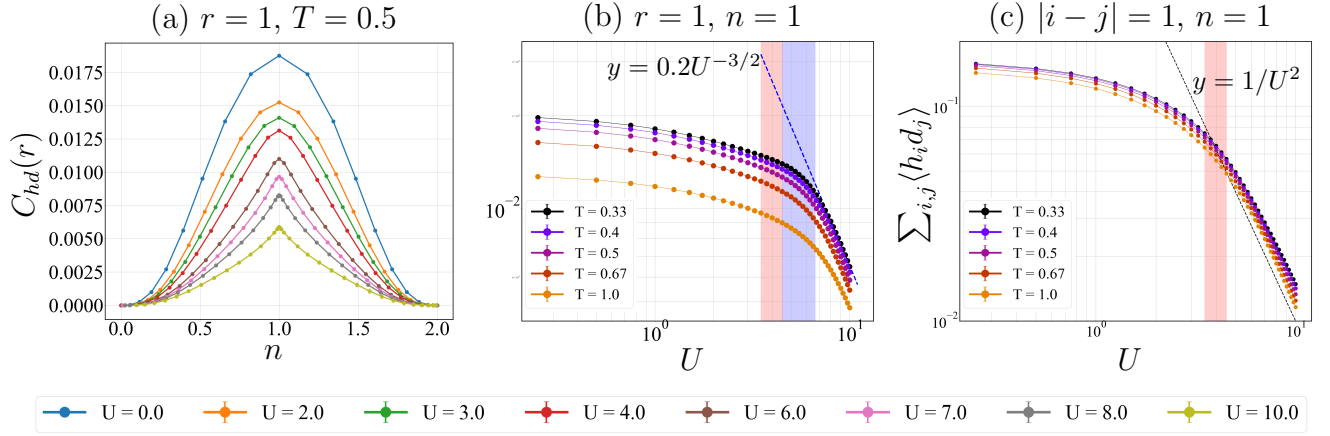


FIG. 4: (a) Nearest neighbor holon doublon correlations at $T/t = 0.5$. The nearest neighbor holon-doublon correlation is always positive, indicating the system prefers to “bunch up” holons and doublons for all U/t and doping, with a maxima at half filling. (b) Nearest neighbor holon doublon correlations at half filling. Holon doublon correlations are monotonically decreasing due to energy cost to form double occupancy from onsite repulsion. Note that beyond the blue shaded region ($U/t \in (4.5, 6.7)$) approximate interval in which $d(T)$ didn’t show a minima in Fig 2), $C_{hd}(1) \sim (U/t)^{-3/2}$ at low temperatures, with the blue dashed line $y = \frac{1}{5U^{3/2}}$. (c) Probability to have a holon doublon pair between nearest sites. In the Mott insulating state, this scales $\sim t^2/U^2$ due to coherent tunneling of singlets [36, 68]. Below the charge crossover window (marked approximately by the red shaded region), coherence is lost, differentiating the nature of ground states on either side of crossover. (All energy scales in the figures are in units of t).

tion; this captures the opening of the Mott gap at half filling. As noted in Ref [67], increasing U/t reduces the double occupancy; near half filling, “freezing” of charges is maximum, resulting in electrons getting pinned down to form local moments which reduces the density-density repulsion. The minima of the local ($r = 0$) and nearest neighbor ($r = 1$) correlations $C_{nn}(r)$ is at $n \approx 0.5$ (and $n \approx 1.5$; because of particle-hole symmetry of the correlator) at large U/t , due to combination of onsite repulsion and Pauli exclusion principle, as noted in Ref [36]. Note that nonlocal correlations (only nearest neighbor density correlation is shown in Fig 3) are always negative, signalling “anti-bunching” or repulsion between non local density pairs.

At half filling, nearest neighbor density correlations steadily decrease in magnitude towards 0 with increasing U/t , due to onsite repulsion, shown in Fig 3 (f). As expected, charges become completely frozen and hence the effective repulsion between nearest neighbor density pairs go to 0 at $U/t \rightarrow \infty$. Density correlations are always decreasing with T/t , as found in Ref [9]. For weak interactions, temperature effects are more prominent, with $|C_{nn}(1)|$ decreasing rapidly as T/t is increased. Strong interactions tend to wash out temperature effects, causing $|C_{nn}(1)|$ to decrease slowly as T/t is increased, a consequence of the Mott insulating state where charges become “frozen”, and hence charges always repel on a length scale shorter than the thermal de Broglie wavelength [67].

B. Doublon-Holon correlation functions

The dominant contribution to density-density correlations at half filling comes from the doublon-holon correlation function:

$$C_{hd}(\mathbf{r}) = \frac{1}{N_s} \sum_{\mathbf{i}} \langle h_{\mathbf{i}+\mathbf{r}} d_{\mathbf{i}} \rangle - \langle h_{\mathbf{i}+\mathbf{r}} \rangle \langle d_{\mathbf{i}} \rangle \quad (6)$$

where the holon and doublon operators are defined in Eq 2. Expanding the density-density correlator as

$$\langle n_{\mathbf{i}} n_{\mathbf{j}} \rangle_C = \langle h_{\mathbf{i}} h_{\mathbf{j}} \rangle_C + \langle d_{\mathbf{i}} d_{\mathbf{j}} \rangle_C - 2 \langle h_{\mathbf{i}} d_{\mathbf{j}} \rangle_C \quad (7)$$

For $U/T \gg 1$, the probability to find holon-holon or doublon-doublon pairs vanishes at half filling (the doublon and holon densities are very small); the density density and holon doublon correlations are thus anti-correlated. The nearest-neighbor holon-doublon correlations are the most dominant ones, and can be detected in site-resolved parity projected experiments [36]. For fermionic systems, these fluctuations occur with a probability of $(t/U)^2$ and are relevant for generating spin singlets between neighboring sites at half filling [68], as shown by expanding the ground state perturbatively in t/U around the state with zero double occupancy. Once formed, the doublon-holon pairs can fluctuate to give rise to singlet pairs between nearest neighbors, and in turn, antiferromagnetic correlations below T_{spin} . Also, binding of doublon-holon pairs have been proposed as a mechanism for Mott transition in the single band Hubbard

model [69–72]. Experimental evaluation of conditional probability of finding a nearby doublon, given a hole at a site shows an enhancement with larger U/t values at half filling, suggesting that such doublon hole pairs are indeed favored in the Mott insulating limit[36]. Note that at all temperatures $T \ll U$ considered here, these fluctuations are strictly quantum in nature.

The doping and U dependence of $C_{hd}(r = 1)$ is shown in Fig 4. Doublon holon pairs always tend to bunch up, since it is always preferable for the system to have a holon next to a doublon to get rid of the double occupancy by fluctuating into a singlet pair between neighboring sites. For small U/t (metallic regime), this is a consequence of getting rid of the Pauli blockade due to double occupancy to favor the hopping of fermions and hence gain in kinetic energy. At large U/t (correlated insulator regime) it is a consequence of both Pauli exclusion and strong on-site repulsion. At half filling, this process is maximized as the number of doublons equal the number of holons. There’s no isolated doublons/holons left once the pairs have been formed; which would have otherwise interacted amongst themselves with an effective repulsion (shown in appendix).

The behavior of $C_{hd}(r)$ at half filling is anti-correlated with that of $C_{nn}(r)$ as seen in the previous section (Fig 3(c)). For nearest neighbors, $C_{hd}(r = 1)$ is a decreasing function of U at half filling due to energy cost to form doublons, shown in Fig 4(b). However, the U/t dependence of $C_{hd}(1)$ differs greatly for small and large U/t , with the transition happening after the charge gap has already formed at the respective temperature. The blue shaded region (in which $\frac{\partial d}{\partial T} > 0$ for all temperatures considered, Fig 2(h)) marks a crossover; in the “metallic” regime, $C_{hd}(1)$ has a weaker U/t dependence. However, on the “insulating” side, $C_{hd}(1)$ shows a much stronger U/t dependence, asymptotic to $\sim U^{-3/2}$ for low temperatures. This likely suggests that the “magnetic” crossover window separates regimes in which singlet pair formation due to doublon holon fluctuations are governed by different mechanisms.

Excitations giving rise to doublon holon pairs also give information about the nature of the ground state. At strong coupling, coherent tunneling of spin singlets between nearest neighbor sites that give rise to doublon holon pairs should scale as $(t/U)^2$ [68]. This is shown in Fig 4 (c), where the probability to form doublon holon pairs between neighboring sites $\langle h_i d_j \rangle$ becomes approximately $(t/U)^2$ in the large U/t (insulating) regime. However, as one approaches the charge gap crossover window (red shaded region), this coherence is lost, and below the gap closing point U_c (from Fig 3(b)), deviation from $(t/U)^2$ behavior signals absence of nearest neighbor singlet pairs in the ground state. This suggests that an opening of charge gap as indicated by number density fluctuations also implies that the system favors a ground state with no double occupancy.

C. Moment moment correlation functions

The local moment (Eq 3) is a central quantity in probing the correlated insulator regime, as it is accessible in parity imaging experiments, [8] where singly occupied sites are detected. The local moment correlation function is defined by

$$C_{mm}(\mathbf{r}) = \frac{1}{N_s} \sum_{\mathbf{i}} \langle \hat{m}_{\mathbf{i}+\mathbf{r}}^2 \hat{m}_{\mathbf{i}}^2 \rangle - \langle \hat{m}_{\mathbf{i}+\mathbf{r}}^2 \rangle \langle \hat{m}_{\mathbf{i}}^2 \rangle \quad (8)$$

Note that according to the definition of Eq 2, the local moment correlation function also obeys the identity,

$$\langle m_{\mathbf{i}}^2 m_{\mathbf{j}}^2 \rangle = \langle n_{\mathbf{i}} n_{\mathbf{j}} \rangle_C + 4 \langle h_{\mathbf{i}} d_{\mathbf{j}} \rangle_C \quad (9)$$

Eq 9 is used to benchmark our numerics, where each correlator is obtained independently from DQMC simulations. Eq 9 also implies that the tendency of the system to pair up local moments between neighboring sites is a competition between repulsive density pairs, and attractive doublon holon pairs. At low doping, “bunching” of doublon and holon pairs are strongly enhanced, whereas density fluctuations are reduced due to an insulating gap beyond a critical $U_c(T)$. This allows the system to have neighboring pairs of local moments that are locked into a singlet state due to the fluctuation of the doublon holon pairs. However, at large doping, the system lies completely inside the lower or the upper Hubbard band (from the thermodynamic DOS $\frac{\partial n}{\partial \mu}$) and density repulsion dominates. This leads to a suppression of the moment moment correlation, becoming minimum in the same doping window as the density density correlator $C_{nn}(r = 1)$. This creates an “optimal” doping window around half filling in which neighboring singlet pair formations are favored; this doping window steadily decreases with U/t (shown in inset of Fig 5(a)), due to increasing energy cost from double occupancy to form attractive doublon holon pairs.

A comparison between $C_{mm}(r = 1)$ (Fig 5(b)) at interaction strength $U > U_c(T)$, shows that the optimal doping window favoring singlet pair formation between neighboring sites is affected minimally with increasing temperature, in the range we consider here. This indicates that the suppression of the singlet formation doping window with increasing U/t , observed in Fig 5(a) and its inset is largely quantum in nature, and happens at temperatures above the spin ordering temperature, at least upto $T = t$. However, $C_{mm}(1)$ only increases upto a critical value of U/t in the correlated insulator regime, and decreases steadily after that, both at and away from half filling. This is in contrast to the behavior of local moments $\langle m_{\mathbf{i}}^2 \rangle$ which get bigger with increasing U/t [73]. Moment correlations are also short range at the temperature range we study; at half filling, moment correlations rapidly go to 0 beyond one lattice spacing.

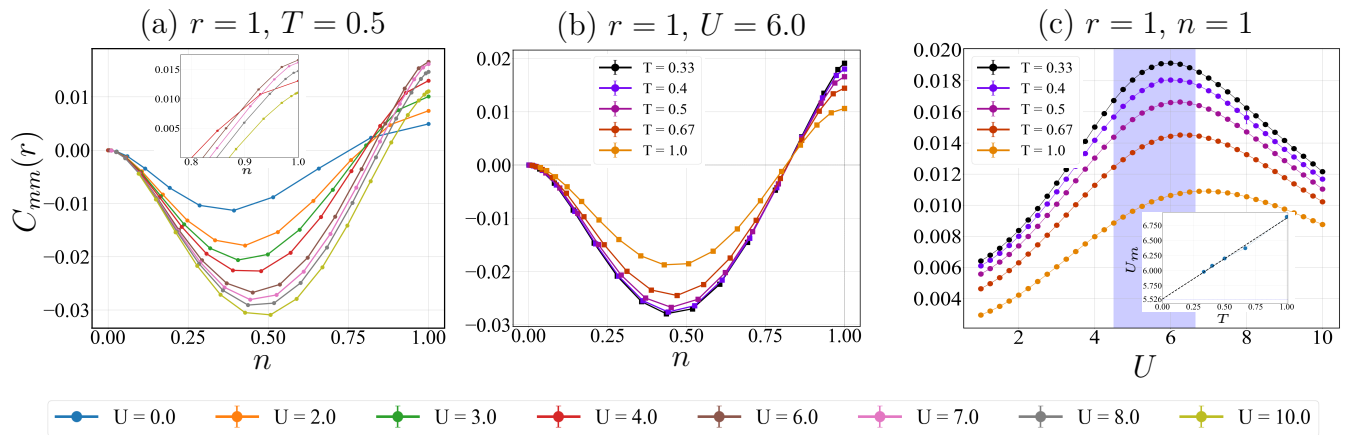


FIG. 5: (a) Nearest neighbor moment moment correlation function $C_{mm}(1)$. Away from half filling, singlet pair formation is suppressed with increasing U/t in the density repulsion dominated region. Near half filling, singlet pairs between nearest neighbor sites are favored due to doublon holon attraction. **Inset:** The doping window in which singlet formation is preferred ($C_{mm}(1) > 0$) decreases monotonically with U , likely due to strong onsite repulsion. (b) $C_{mm}(1)$ at a fixed U/t for multiple temperatures. The doping window over which singlet pair formation is favored is independent of temperature, indicating that the suppression of the optimal doping window with increasing U/t is strictly quantum in nature. (c) $C_{mm}(1)$ at half filling. Although the density density correlation function, $C_{nn}(1)$ and holon doublon correlation function $C_{hd}(1)$ are monotonic functions of U/t , $C_{mm}(1)$ exhibits a peak in the interval $U/t \in (4.5, 6.7)$. This is in contrast to $\langle m^2 \rangle$ which grows with increasing U/t . **Inset:** Location of maximum of $C_{mm}(1)$, $U_m(T)$ depends linearly on T , with low temperature extrapolated values very close to the first order transition line in Ref [20]. (All energy scales in the figures are in units of t).

To study how the crossover windows introduced in Sec III influences the development of short range local moment correlations, we calculate $C_{mm}(1)$ at half filling for various temperatures, shown in Fig 5(c). Note that the local moment correlations peak at an interaction strength higher than the charge gap opening scale U_c at the respective temperature. The maxima in $C_{mm}(1)$ shifts to lower U/t with lowering temperature, similar to zero crossings of $\frac{\partial \bar{\kappa}}{\partial T}$. In the weak U/t limit, doublon holon attractions, $C_{hd}(1)$ are dominating, resulting in initial increase of $C_{mm}(1)$ with U/t . However, in the large U/t limit, $C_{mm}(1)$ decreases due to weakening of $C_{hd}(1)$ from strong onsite repulsion with increasing U/t . Short range correlations are important in generating pseudogap[74–77]; in the intermediate temperature range, the critical interaction strength at which Ref [78] reported pseudogap onset is in very favourable agreement with $U_m(T)$, the location of peak of $C_{mm}(1)$ in our work in the appropriate temperature range. This likely suggests that pseudogap onset can be associated with maximizing short range moment correlations that follows after the opening of charge gap.

Previous CDMFT work on the nature of Metal-Insulator transition [20] had also found a coexistence region at low temperature ($T \approx 0.01t$) where both the metallic and insulator solution shows a large scattering rate at $(\pi, 0)$ orbital; responsible for opening the single particle gap. As noted in previous DMFT studies, exclusion of the antiferromagnetic dome can reveal a first order Metal-Insulator transition[19]; in this spirit, ignoring competing ordering mechanisms at lower tem-

peratures allows us to safely extrapolate the peak behavior of $C_{mm}(1)$ to lower temperatures. The magnitude of $U_m(T)$ (details about extracting $U_m(T)$ given in appendix) shows a linear dependence on T , reaching $U_m \sim 5.5t$ at very low temperatures (shown in inset). Our extrapolated value of $U_m(T)$ to the low temperatures considered in Ref [20] ($T \sim 0.01t$), is exactly in the middle of the coexistence region; suggesting that nearest neighbor moment correlations are strongest there and are indeed driving the divergence of the scattering rate. This implies that the peaks observed in $C_{mm}(1)$ in Fig 5(c) is likely a higher temperature extension of the mechanism driving the phase coexistence and an “anomalous metal” to develop below the critical point (U_{MIT}, T_{MIT})[20].

V. NON LOCAL CORRELATIONS BEYOND NEAREST NEIGHBOR

With advances in cold atom experiments, measurements of non local correlations beyond the first nearest neighbor are possible, although these might be orders of magnitude smaller than the nearest neighbor correlations[8, 16, 46]. Since different correlation functions show different behavior as function of U/t and doping, we look at all possible independent next nearest neighbor correlations (between same sublattice, C^{A-A}) between density, holon and doublon pairs. We show only density density, holon doublon, and doublon doublon correlators in Fig 6, as every other correlator can be derived from them due to the constraints in Eq 2 or particle hole

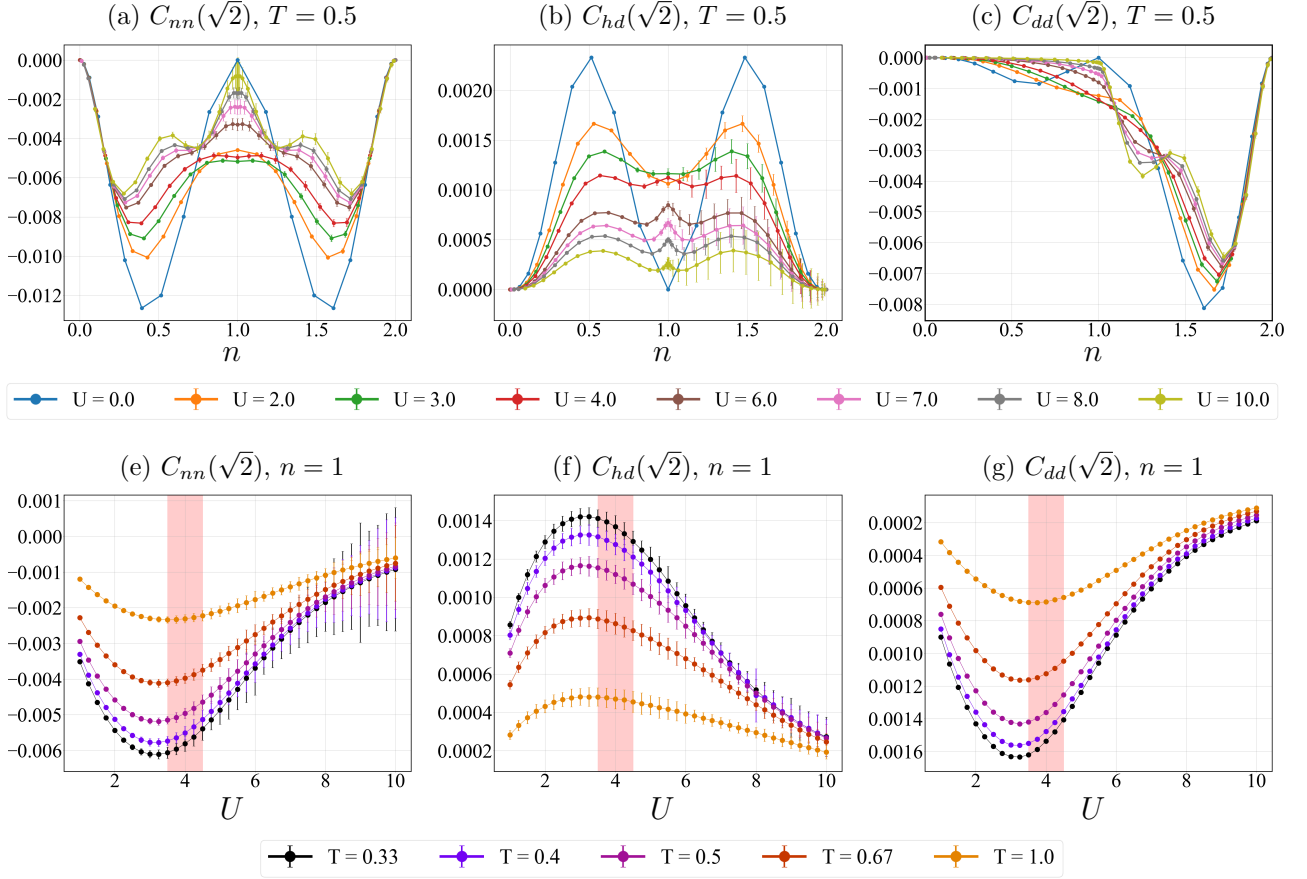


FIG. 6: Next nearest neighbor correlations C^{A-A} between same sublattice sites A on a square lattice. **Top panel:** (a) Density density correlator $C_{nn}(\sqrt{2})$ (b) Holon doublon correlator $C_{hd}(\sqrt{2})$ (c) Doublon doublon correlator $C_{dd}(\sqrt{2})$ at multiple U/t , $T/t = 0.5$. Note that the correlations show distinct behavior before and after opening of a charge gap, through presence of additional minima/maxima at intermediate doping on the correlated insulator side. **Bottom panel:** (d) Density density correlator (e) Holon doublon correlator (f) Doublon doublon correlator at half filling. A minima in the density density correlator was shown to exist in the crossover window [61]. However, such minima/maxima exists below the charge crossover window (red shaded region) for all correlation functions between density, holon and doublon pairs, and persists for all temperatures studied here. (All energy scales in the figures are in units of t).

transformation .

As noted before, increasing U/t beyond a critical value $U_c(T)$ opens up a Mott gap, as seen in Fig 3. A common feature across all the correlators in the top panel is the presence of a single minima/maxima in the metallic regime, and the appearance of multiple minima/maxima (on the appropriate hole/particle doped side) after the charge gap has opened up. For the density density and doublon doublon correlations, a shoulder develops on crossing $U_c(T)$, that turns into a secondary minima with increasing U/t , while pushing the primary minima away from the doping where it peaked in the metallic regime. For the holon-doublon correlations, a minima at half filling changes into a local maxima, whose peak decreases with increasing U/t . This is shown in Fig 6 top panel, for a fixed temperature of $T/t = 0.5$. Since these features are seen universally across all correlators in the charge sector, we can speculate that this might be tied to appear-

ance of an upper and lower Hubbard band with strong interactions after a charge gap has opened up in the thermodynamic density of states; as opposed to a single band for the metallic regime (Fig 2). The exact reason why the next nearest neighbor correlations show this behavior is not clear to us.

Next nearest neighbor correlation functions at half filling also show a non monotonic behavior with respect to U/t at all temperatures studied here, shown in Fig 6 bottom panel. All the correlation functions have either a maxima or a minima near the crossover window extracted from $\frac{\partial \kappa}{\partial T}$ (Fig 3). Such a behavior was reported from diagrammatic Monte Carlo study at half filling for the density density correlation function [61]; however other correlation functions associated with the charge sector also show a similar behavior. The repulsive density density and doublon doublon correlation functions steadily decrease to a minima before the crossover window, and

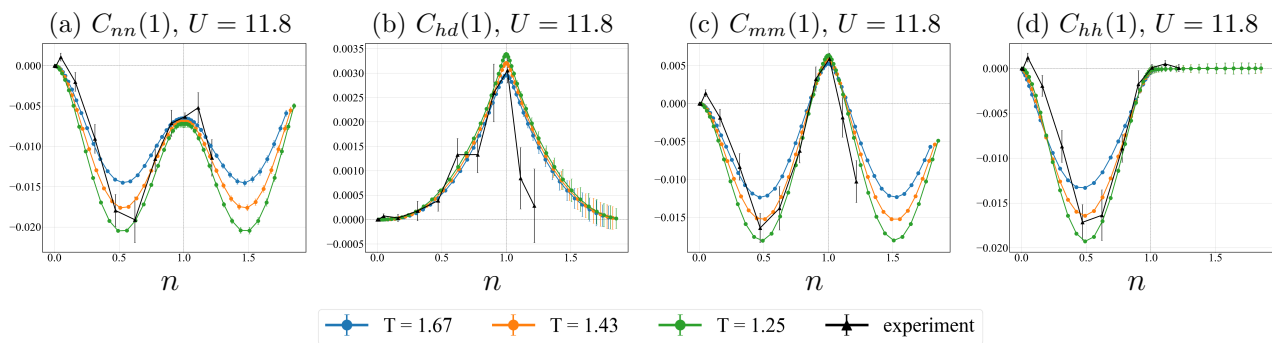


FIG. 7: Comparison of experimental nearest neighbor correlation functions [36] with QMC simulations at $U/t = 11.8$ (a) Density density correlation function. (b) Holon doublon correlation function. (c) Moment moment correlation function. (d) Holon holon correlation function. The temperature estimate of the experimental data is $T/t \approx 1.43$, by comparing with QMC data, which is lower than the temperature considered ($T/t = 1.6$) in Ref [36] for comparing equation of state data with Ref [64], and higher than the ones obtained by fluctuation thermometry, $T/t \sim 0.69$. The QMC data is shown by circles, and the experimental data by black triangles. (All energy scales in the figures are in units of t).

increases through the metal-insulator crossover with increasing U/t , saturating to 0 as $U/t \rightarrow \infty$. Similarly, the doublon holon attractions peak before the charge gap opens up, and steadily decreases with increasing U/t . Tracking any of these correlation functions in experiments can qualitatively capture the crossover from metallic to correlated insulator regime, in addition to number density fluctuations.

VI. COMPARISON WITH EXPERIMENTAL DATA

In this section, we compare our numerical results with experimental findings from a cold atomic Fermi gas, subjected to Hubbard like interactions in an optical trap. Correlation functions and thermodynamics are observed by a bilayer quantum gas microscope capable of site resolved density readout of the gas in 2D in a single fluorescence image [36]. Imaging a large number of sites gives access to equation of state, and local and nonlocal correlation functions between density, doublon, holon and singlon pairs. The temperature of the gas can be determined by simultaneously measuring the compressibility and total density fluctuations, together with the fluctuation dissipation theorem, Eq 5. Although the experiment measurements are performed at $U/t \approx 7.1, 11.8, 18.3, 25.5$, we only show the correlators at $U/t = 11.8$. Fluctuation thermometry of the gas yields $T/t = 0.69$ for $U/t = 11.8$ [36], however, this is in contrast with the temperature estimation by DQMC.

We estimate the temperature by fitting correlation functions obtained experimentally, with DQMC results at multiple temperatures. For $U/t = 11.8$, we compare the experimental data to correlators in the temperature range $T/t = 1.25, 1.43, 1.67$. This is shown in Fig 7 (a)-(d). Out of the three temperatures, the experimental data seem to agree best with the numerical results at

$T/t = 1.43$. This is slightly lower than the $T/t = 1.6$ used to compare the experimental equation of state data [36] to DQMC calculations from [64].

VII. CONCLUSION

In this work, we have looked at equal time correlation functions in the repulsive Fermi Hubbard model on a square lattice, that can be measured in cold atom experiments. Our analysis shows a way to isolate crossover between a band like (metallic) description to local moment like (correlated insulator) description as a function of U/t , which is analogous to the BEC-BCS crossover in the attractive U case, both at and away from half filling. Temperature dependence of the charge gap shows crossover between band regime and local moment regime in $U/t \in (3.5, 4.5)$ in the temperature ranges considered here; the crossover window is much lower than the interaction scale at which moderate range antiferromagnetic correlations are expected to be maximal, $U/t \approx 8$, and lower than the U_{MIT} estimated by DMFT studies [67]. Complemented with temperature dependence of average doublon number, this helps identify various phases in the $U - \mu$ plane at fixed T , across which correlation functions can be studied. While thermodynamic quantities like compressibility and specific heat can capture the metal-insulator crossover, correlation functions can also track such behavior equally well.

In the charge sector, density density correlations and holon doublon correlations are the most important processes, as other correlation functions can be derived as competition between these two processes. Nearest neighbor singlet pair formation is determined by competition between repulsive density pairs and attractive doublon holon pairs, and interplay between local moment, doublon, and holons in terms of their equal time correlation functions show signatures on crossover from the metal-

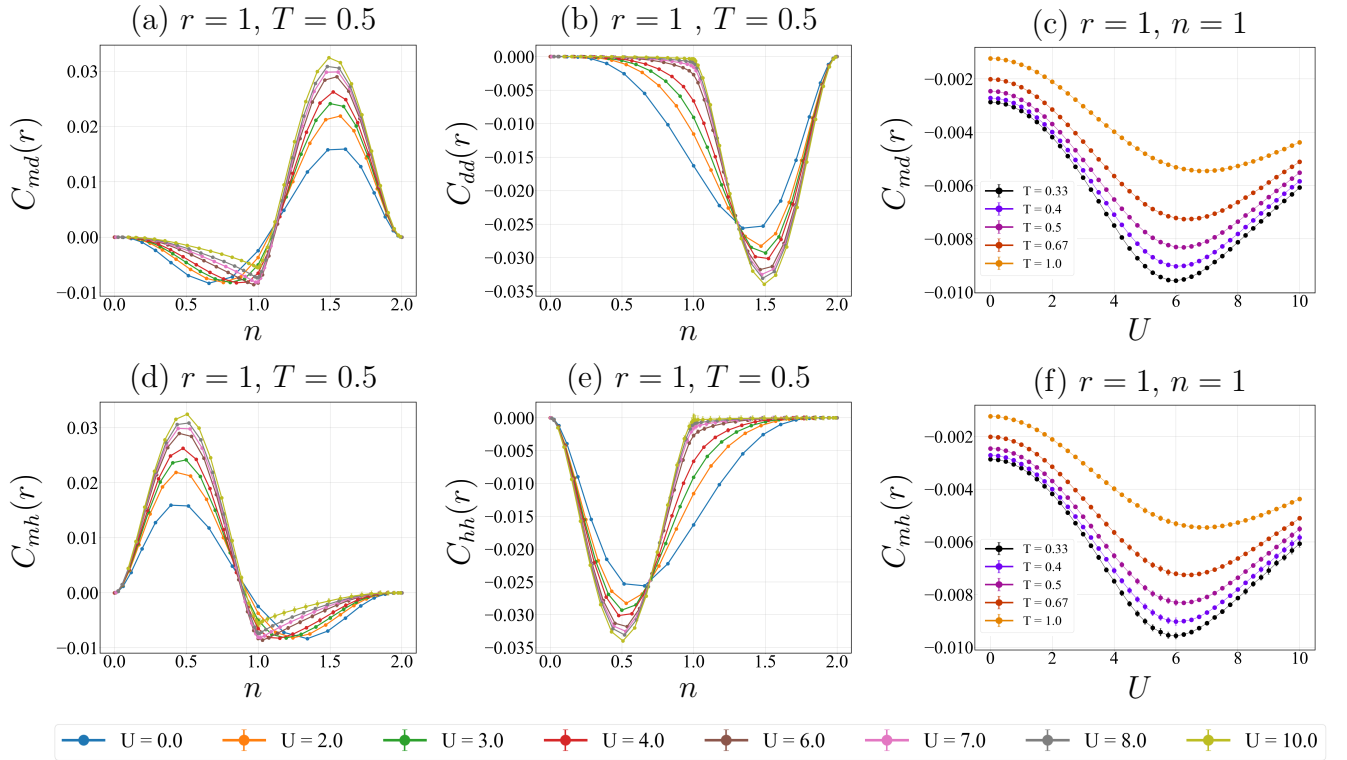


FIG. 8: Moment doublon correlations, $C_{md}(r)$ and Moment holon correlations, $C_{mh}(r)$ in the Hubbard model. **Top panel (a)** Nearest neighbor moment doublon correlation function $C_{md}(1)$. At half filling, it is suppressed as the system favors neighboring pairs of doublon holon fluctuating into singlets pairs. In the particle doped side, it is favored as the system tries to have a local moment between two doublons to minimize doublon doublon repulsion. **(b)** Nearest neighbor doublon doublon correlation functions $C_{dd}(1)$. In the metallic regime, (below $U/t \sim 4.0$) there is finite repulsion between nearby doublon pairs at half filling. In the correlated insulator regime, this goes to 0 due to depletion of double occupancy. **(c)** $C_{md}(1)$ at half filling. Note that this has the same non monotonic behaviour as $C_{mm}(1)$ with respect to U/t . **Bottom panel (d)** Nearest neighbor moment holon correlation function $C_{mh}(1)$. At half filling, it is suppressed due to doublon holon fluctuations, in the hole doped side, it is positive due to hole hole repulsion. **(e)** Nearest neighbor holon holon correlation function $C_{hh}(1)$. In the metallic regime, there is finite repulsion between neighboring holons at half filling, in the correlated insulator regime, this goes to 0 at half filling due to depletion of holes. **(f)** $C_{mh}(1)$ at half filling, showing similar behavior as $C_{md}(1)$. (All energy scales in the figures are in units of t).

lic to the correlated insulator regime, both at and away from half filling. An analytical understanding of the signatures of crossover from the band to local moment regime through the next nearest neighbor correlations is an open question. In light of recent progress in fluorescence imaging with quantum gas microscopes, these correlation functions can be experimentally observed, and can serve as benchmarks and guide experimental investigation into the intermediate temperature phases in the 2D repulsive Hubbard model.

VIII. ACKNOWLEDGEMENT

We would like to thank Thomas Hartke, Ningyuan Jia and Martin Zweirlein for providing data on various correlation functions in Fig 7. We would also like to thank Abhisek Samanta for feedback on the manuscript and numerous insightful discussions. S.R and N.T would like

to acknowledge support from National Science foundation through grant number NSF-DMR grant no 2138905. T.P. acknowledges financial support from Fundação Carlos Chagas Filho de Amparo à Pesquisa do Estado do Rio de Janeiro grant numbers E-26/200.959/2022 and E-26/210.100/2023; CNPq grant numbers, 403130/2021-2 and 308335/2019-8; and also INCT-IQ. Numerical calculations have been carried out using high-performance computing resources of the Unity cluster at Ohio State University.

Appendix A: Moment holon and Moment Doublon correlation functions

From the definition of doublons, holons and local moments Eq 2, one can rewrite the moment moment correlation function as

$$\begin{aligned}
C_{mm}(\mathbf{r}) &= \sum_{|\mathbf{i}-\mathbf{j}|=r} \langle m_{\mathbf{i}}^2(1-h_{\mathbf{j}}-d_{\mathbf{j}}) \rangle - \langle m_{\mathbf{i}}^2 \rangle \langle 1-h_{\mathbf{j}}+d_{\mathbf{j}} \rangle \\
&= \sum_{|\mathbf{i}-\mathbf{j}|=r} \langle m_{\mathbf{i}}^2 d_{\mathbf{j}} \rangle - \langle m_{\mathbf{i}}^2 \rangle \langle d_{\mathbf{j}} \rangle + \langle m_{\mathbf{i}}^2 h_{\mathbf{j}} \rangle - \langle m_{\mathbf{i}}^2 \rangle \langle h_{\mathbf{j}} \rangle \\
&= -[C_{md}(\mathbf{r}) + C_{mh}(\mathbf{r})] \tag{A1}
\end{aligned}$$

The moment doublon and moment holon correlations, as defined in Eq A1 are thus anticorrelated with moment moment correlations. We would like to note the similarity between the correlators defined in Eq A1 and the antimoment correlation functions observed experimentally in Ref [8, 46] and simulated in Ref [79]. The similarity stems from the constraint that locally on each site, there can be either a holon, a doublon or a local moment.

Nearest neighbor moment holon (moment doublon) correlations include fluctuations in which adjacent moments and holons(doublons) swap positions. At half filling, strong onsite repulsion at large U/t would force single occupancy(moment formation) on every site locally. On particle(hole) doping, one creates local puddles of doublons(holons), that can fluctuate with a nearby local moment. The doublon(holon) can then move through the entire lattice by these fluctuations, thus destroying neighboring moment correlations entirely.

Fig 8 shows the behavior of $C_{md}(r=1)$ and $C_{mh}(r=1)$ with respect to interaction strength at $T/t = 0.5$. Note that below $U/t \sim 4$, in the metallic regime, the minima of $C_{md}(r=1)$ and $C_{mh}(r=1)$ are away from half filling on the hole doped and particle doped side respectively. On entering correlated insulator regime, the minima shifts towards half filling. This is a consequence of presence of finite number of doublons and holons in the band limit, which quickly decreases with increasing interaction in the correlated insulator regime. Presence of finite number of doublon/holon pairs at half filling in the metallic regime also show up in the behavior of doublon doublon $C_{dd}(r=1)$ and holon holon $C_{hh}(r=1)$ correlators.

Both the moment doublon and moment holon correlations exhibit nontrivial sign changes at finite doping, Fig A1(a) and (d). Note that the moment doublon and moment holon correlations can be rewritten as

$$\begin{aligned}
\langle m_{\mathbf{i}}^2 d_{\mathbf{j}} \rangle_C &= -[\langle h_{\mathbf{i}} d_{\mathbf{j}} \rangle_C + \langle d_{\mathbf{i}} d_{\mathbf{j}} \rangle_C] \\
\langle m_{\mathbf{i}}^2 h_{\mathbf{j}} \rangle_C &= -[\langle h_{\mathbf{i}} d_{\mathbf{j}} \rangle_C + \langle h_{\mathbf{i}} h_{\mathbf{j}} \rangle_C] \tag{A2}
\end{aligned}$$

which shows that the moment doublon(holon) correlations are competition between attractive holon doublon pairs and repulsive doublon doublon (holon holon) pairs. This is similar to the behavior noted in Ref [61].

In the metallic regime, there is finite repulsion between doublon pairs $C_{dd}(r=1)$ and holon pairs $C_{hh}(r=1)$ at half filling, which competes with the attraction between doublon and holon pairs, the latter being most dominant at half filling. In the correlated insulator regime, the

repulsion between doublon pairs and holon pairs are essentially 0 at half filling. The dominant contributions are due to $C_{hd}(r=1)$; hence $C_{md}(r=1)$ and $C_{mh}(r=1)$ are negative. However, on the hole doped side, holon-holon repulsions force the system to prefer singly occupied sites between holon pairs, which causes $C_{mh}(r=1)$ to be positive (and vice versa for $C_{md}(r=1)$ on the particle doped side). At half filling, both $C_{mh}(r=1)/C_{md}(r=1)$ exhibit the same non monotonic nature as $C_{mm}(r=1)$.

Appendix B: Sign problem

In QMC, the partition function is expressed as a product of determinants of fermionic up and down spins, weighted over a path in the phase space of auxiliary Ising like spins, $\{s\}$;

$$Z = \left(\frac{1}{2}\right)^{NM} \sum_{\{s\}} \text{Det}O_{\uparrow}(\{s\}) \cdot \text{Det}O_{\downarrow}(\{s\}) \tag{B1}$$

where N is the number of lattice sites, and M is chosen to minimize trotter error due to step size in imaginary time, $\Delta\tau = \beta/M$. The Markov chain proceeds by selecting a new configuration, and accepting the new move based on detailed balance. The Boltzmann weight/probability of a particular configuration $\{s\}$ in the partition function is

$$p(\{s\}) = \text{Det}O_{\uparrow}(\{s\}) \cdot \text{Det}O_{\downarrow}(\{s\}) \tag{B2}$$

The above weight might not always be positive, and hence cannot be treated as a classical probability. This leads to the ‘‘sign problem’’ in QMC. The expectation value of observables have to be re-weighted by the sign of determinants

$$\langle A \rangle = \frac{\sum_{\{s\}} p(\{s\}) A(\{s\})}{\sum_{\{s\}} p(\{s\})} = \frac{\sum_{\{s\}} |p(\{s\})| A(\{s\})}{\sum_{\{s\}} |p(\{s\})| \text{sign}(\{s\})} \tag{B3}$$

The quantity in the denominator is the average sign of the QMC simulation, and can become very small at low temperatures, or large number of lattice sites, $\langle \text{sign} \rangle \propto e^{-\beta N_s}$. We provide the behavior of the average sign for the 10×10 lattice used in the simulation, at $T/t = 0.5, 0.4$ in Fig 9. Note that for reporting correlators and thermodynamic variables, we have stuck to cases where the average sign ≥ 0.5 .

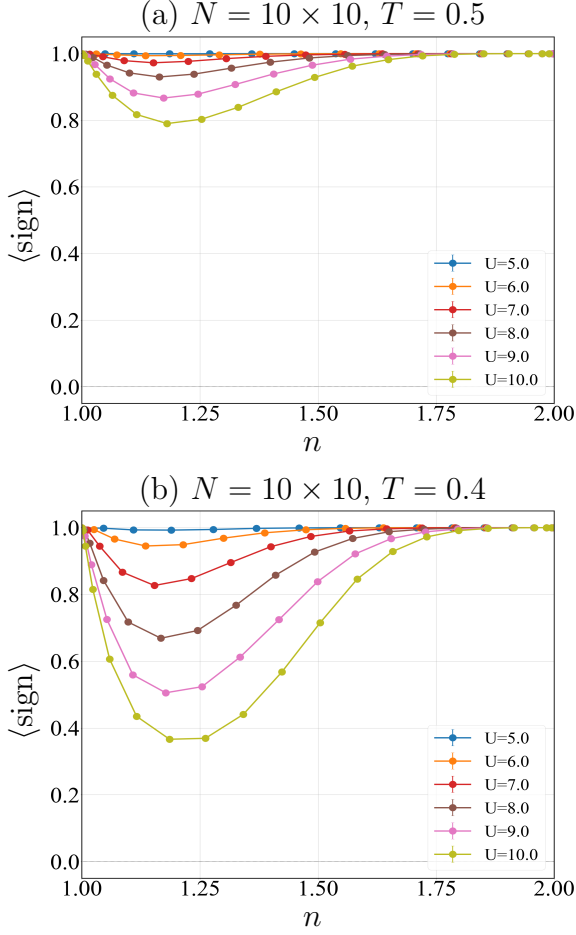


FIG. 9: Average sign of fermionic determinants in DQMC for 10×10 lattice for different U/t . (a) $T/t = 0.5$, (b) $T/t = 0.4$. The imaginary time step size is chosen to be $\Delta\tau = 0.05$.

Appendix C: Moment Moment correlation functions

The moment moment correlation functions are extremely short ranged, in the temperature window we study. We show the next nearest neighbor moment moment correlation between the same sub lattice (A-A) sites in Fig 10 top panel. In the metallic regime, before the charge gap has opened up, next nearest neighbor moment moment correlation is suppressed at half filling; however, correlations almost vanish once the charge gap has opened up. Correlations at finite doping shows more complicated behavior; strong suppression persists at $n \sim 0.25, 1.75$. However, once the charge gap has opened up, a secondary minima starts to develop, and correlations are suppressed closer to half filling as well. Note that the suppression of correlations near half filling, above the charge gap, is in line with secondary minima/maximas appearing in other correlation functions, as noted in the main text (Fig 6).

We also show the polynomial fits to QMC data used

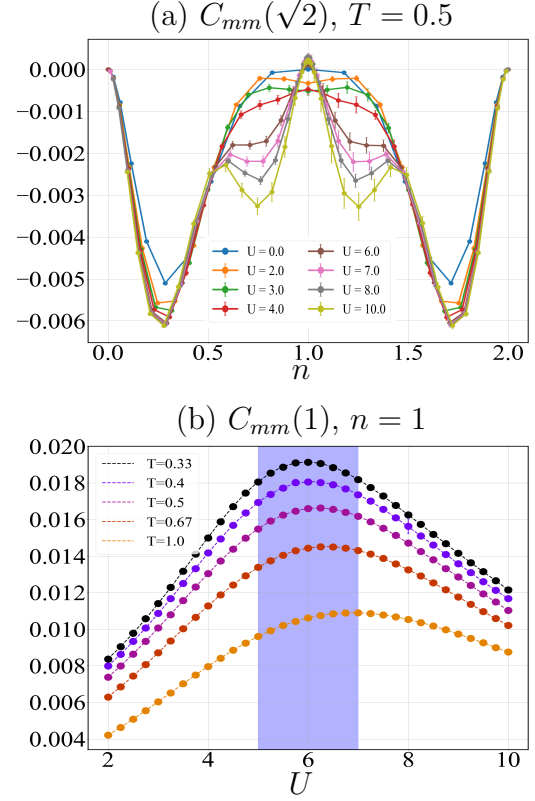


FIG. 10: (a) Next nearest neighbor moment moment correlation functions $C_{mm}(\sqrt{2})$ at $T/t = 0.5$. Note that in the metallic regime, there is a single minima in the particle/hole doped side, with finite repulsion between moment pairs on next nearest neighbor sites. On crossover to the insulating regime, $U/t \sim 4$, the primary minimas give away to secondary minimas at doping close to half filling. The repulsion between the moment pairs quickly die to 0 with increasing U/t . Next (b) Nearest neighbor moment moment correlation functions $C_{mm}(1)$ from QMC, at half filling. The circles with errorbars represent the QMC data points at different temperatures, the dashed lines represent polynomial fit at respective temperature. The blue shaded region denotes the approximate U/t interval in which $C_{mm}(1)$ peaks. (All energy scales in the figures are in units of t).

to obtain the temperature dependence of $U_m(T)$ (interaction strength at which nearest neighbor moment moment correlations $C_{mm}(1)$ peak at half filling at a temperature T), in we fit the data with a 10th order polynomial, in the interval $U \in [2.0, 10.0]$, to capture the tails on both the metallic and insulator regime. The fit is shown at each temperature with dashed line, along with the QMC data (circles). The blue shaded region shows the approximate interaction window in which $C_{mm}(1)$ peaks across different temperatures. This is the “magnetic” crossover window that overlaps with the fan shaped region in Fig 2(h), where $\frac{\partial d}{\partial T} > 0$.

- [1] M. C. Gutzwiller, Effect of correlation on the ferromagnetism of transition metals, *Physical Review Letters* **10**, 159 (1963).
- [2] J. Kanamori, Electron correlation and ferromagnetism of transition metals, *Progress of Theoretical Physics* **30**, 275 (1963).
- [3] J. Hubbard, Electron correlations in narrow energy bands iii. an improved solution, *Proceedings of the Royal Society of London. Series A. Mathematical and Physical Sciences* **281**, 401 (1964).
- [4] P. W. Anderson, Experimental constraints on the theory of high- T_c superconductivity, *Science* **256**, 1526 (1992).
- [5] M. Qin, T. Schäfer, S. Andergassen, P. Corboz, and E. Gull, The hubbard model: A computational perspective, *Annual Review of Condensed Matter Physics* **13**, 275 (2022).
- [6] E. Cocchi, L. A. Miller, J. H. Drewes, M. Koschorreck, D. Pertot, F. Brennecke, and M. Köhl, Equation of state of the two-dimensional hubbard model, *Physical review letters* **116**, 175301 (2016).
- [7] D. Greif, M. F. Parsons, A. Mazurenko, C. S. Chiu, S. Blatt, F. Huber, G. Ji, and M. Greiner, Site-resolved imaging of a fermionic mott insulator, *Science* **351**, 953 (2016).
- [8] L. W. Cheuk, M. A. Nichols, K. R. Lawrence, M. Okan, H. Zhang, and M. W. Zwierlein, Observation of 2d fermionic mott insulators of $k \approx 40$ with single-site resolution, *Physical review letters* **116**, 235301 (2016).
- [9] J. Drewes, E. Cocchi, L. Miller, C. Chan, D. Pertot, F. Brennecke, and M. Köhl, Thermodynamics versus local density fluctuations in the metal–mott-insulator crossover, *Physical review letters* **117**, 135301 (2016).
- [10] M. F. Parsons, A. Mazurenko, C. S. Chiu, G. Ji, D. Greif, and M. Greiner, Site-resolved measurement of the spin-correlation function in the fermi-hubbard model, *Science* **353**, 1253 (2016).
- [11] J. Drewes, L. Miller, E. Cocchi, C. Chan, N. Wurz, M. Gall, D. Pertot, F. Brennecke, and M. Köhl, Antiferromagnetic correlations in two-dimensional fermionic mott-insulating and metallic phases, *Physical review letters* **118**, 170401 (2017).
- [12] P. T. Brown, D. Mitra, E. Guardado-Sanchez, P. Schauß, S. S. Kondov, E. Khatami, T. Paiva, N. Trivedi, D. A. Huse, and W. S. Bakr, Spin-imbalance in a 2d fermi-hubbard system, *Science* **357**, 1385 (2017).
- [13] M. A. Nichols, L. W. Cheuk, M. Okan, T. R. Hartke, E. Mendez, T. Senthil, E. Khatami, H. Zhang, and M. W. Zwierlein, Spin transport in a mott insulator of ultracold fermions, *Science* **363**, 383 (2019).
- [14] P. T. Brown, D. Mitra, E. Guardado-Sanchez, R. Nourafkan, A. Reymbaut, C.-D. Hébert, S. Bergeron, A.-M. Tremblay, J. Kokalj, D. A. Huse, *et al.*, Bad metallic transport in a cold atom fermi-hubbard system, *Science* **363**, 379 (2019).
- [15] E. Guardado-Sanchez, A. Morningstar, B. M. Spar, P. T. Brown, D. A. Huse, and W. S. Bakr, Subdiffusion and heat transport in a tilted two-dimensional fermi-hubbard system, *Physical Review X* **10**, 011042 (2020).
- [16] A. Mazurenko, C. S. Chiu, G. Ji, M. F. Parsons, M. Kanász-Nagy, R. Schmidt, F. Grusdt, E. Demler, D. Greif, and M. Greiner, A cold-atom fermi–hubbard antiferromagnet, *Nature* **545**, 462 (2017).
- [17] J. Koepsell, J. Vijayan, P. Sompet, F. Grusdt, T. A. Hilker, E. Demler, G. Salomon, I. Bloch, and C. Gross, Imaging magnetic polarons in the doped fermi–hubbard model, *Nature* **572**, 358 (2019).
- [18] W. F. Brinkman and T. M. Rice, Application of gutzwiller’s variational method to the metal-insulator transition, *Physical Review B* **2**, 4302 (1970).
- [19] L. Fratino, P. Semon, M. Charlebois, G. Sordi, and A.-M. Tremblay, Signatures of the mott transition in the antiferromagnetic state of the two-dimensional hubbard model, *Physical Review B* **95**, 235109 (2017).
- [20] H. Park, K. Haule, and G. Kotliar, Cluster dynamical mean field theory of the mott transition, *Physical review letters* **101**, 186403 (2008).
- [21] Y. Feng, Y. Wang, D. M. Silevitch, S. E. Cooper, D. Mandrus, P. A. Lee, and T. Rosenbaum, A continuous metal-insulator transition driven by spin correlations, *Nature Communications* **12**, 2779 (2021).
- [22] R. Zhang, Q. Fu, C. Yin, C. Li, X. Chen, G. Qian, C. Lu, S. Yuan, X. Zhao, and H. Tao, Understanding of metal-insulator transition in vo_2 based on experimental and theoretical investigations of magnetic features, *Scientific reports* **8**, 17093 (2018).
- [23] S. Ricco, M. Kim, A. Tamai, S. McKeown Walker, F. Y. Bruno, I. Cucchi, E. Cappelli, C. Besnard, T. K. Kim, P. Dudin, *et al.*, In situ strain tuning of the metal-insulator-transition of ca_2ru_4 in angle-resolved photoemission experiments, *Nature communications* **9**, 4535 (2018).
- [24] A. Richardella, P. Roushan, S. Mack, B. Zhou, D. A. Huse, D. D. Awschalom, and A. Yazdani, Visualizing critical correlations near the metal-insulator transition in $ga_1-x mn_x as$, *science* **327**, 665 (2010).
- [25] I. Bloch, J. Dalibard, and W. Zwerger, Many-body physics with ultracold gases, *Reviews of modern physics* **80**, 885 (2008).
- [26] I. Bloch, Ultracold quantum gases in optical lattices, *Nature physics* **1**, 23 (2005).
- [27] I. Bloch, J. Dalibard, and S. Nascimbene, Quantum simulations with ultracold quantum gases, *Nature Physics* **8**, 267 (2012).
- [28] W. S. Bakr, J. I. Gillen, A. Peng, S. Fölling, and M. Greiner, A quantum gas microscope for detecting single atoms in a hubbard-regime optical lattice, *Nature* **462**, 74 (2009).
- [29] M. Aidelsburger, M. Atala, M. Lohse, J. T. Barreiro, B. Paredes, and I. Bloch, Realization of the hofstadter hamiltonian with ultracold atoms in optical lattices, *Physical review letters* **111**, 185301 (2013).
- [30] C. Gross and I. Bloch, Quantum simulations with ultracold atoms in optical lattices, *Science* **357**, 995 (2017).
- [31] C. Weitenberg, M. Endres, J. F. Sherson, M. Cheneau, P. Schauß, T. Fukuhara, I. Bloch, and S. Kuhr, Single-spin addressing in an atomic mott insulator, *Nature* **471**, 319 (2011).
- [32] J. F. Sherson, C. Weitenberg, M. Endres, M. Cheneau, I. Bloch, and S. Kuhr, Single-atom-resolved fluorescence imaging of an atomic mott insulator, *Nature* **467**, 68 (2010).
- [33] M. Greiner, O. Mandel, T. Esslinger, T. W. Hänsch, and

- I. Bloch, Quantum phase transition from a superfluid to a mott insulator in a gas of ultracold atoms, *nature* **415**, 39 (2002).
- [34] M. Aidelsburger, M. Lohse, C. Schweizer, M. Atala, J. T. Barreiro, S. Nascimbene, N. Cooper, I. Bloch, and N. Goldman, Measuring the chern number of hofstadter bands with ultracold bosonic atoms, *Nature Physics* **11**, 162 (2015).
- [35] M. Boll, T. A. Hilker, G. Salomon, A. Omran, J. Nespolo, L. Pollet, I. Bloch, and C. Gross, Spin-and density-resolved microscopy of antiferromagnetic correlations in fermi-hubbard chains, *Science* **353**, 1257 (2016).
- [36] T. Hartke, B. Oreg, N. Jia, and M. Zwierlein, Doublon-hole correlations and fluctuation thermometry in a fermi-hubbard gas, *Physical Review Letters* **125**, 113601 (2020).
- [37] J. Koepsell, S. Hirthe, D. Bourgund, P. Sompet, J. Vijayan, G. Salomon, C. Gross, and I. Bloch, Robust bilayer charge pumping for spin-and density-resolved quantum gas microscopy, *Physical Review Letters* **125**, 010403 (2020).
- [38] S. Hirthe, T. Chalopin, D. Bourgund, P. Bojović, A. Bohrdt, E. Demler, F. Grusdt, I. Bloch, and T. A. Hilker, Magnetically mediated hole pairing in fermionic ladders of ultracold atoms, *Nature* **613**, 463 (2023).
- [39] G. Salomon, J. Koepsell, J. Vijayan, T. A. Hilker, J. Nespolo, L. Pollet, I. Bloch, and C. Gross, Direct observation of incommensurate magnetism in hubbard chains, *Nature* **565**, 56 (2019).
- [40] J. Vijayan, P. Sompet, G. Salomon, J. Koepsell, S. Hirthe, A. Bohrdt, F. Grusdt, I. Bloch, and C. Gross, Time-resolved observation of spin-charge deconfinement in fermionic hubbard chains, *Science* **367**, 186 (2020).
- [41] J. Koepsell, D. Bourgund, P. Sompet, S. Hirthe, A. Bohrdt, Y. Wang, F. Grusdt, E. Demler, G. Salomon, C. Gross, *et al.*, Microscopic evolution of doped mott insulators from polaronic metal to fermi liquid, *Science* **374**, 82 (2021).
- [42] P. Sompet, S. Hirthe, D. Bourgund, T. Chalopin, J. Bibo, J. Koepsell, P. Bojović, R. Verresen, F. Pollmann, G. Salomon, *et al.*, Realizing the symmetry-protected haldane phase in fermi-hubbard ladders, *Nature* **606**, 484 (2022).
- [43] C. S. Chiu, G. Ji, A. Mazurenko, D. Greif, and M. Greiner, Quantum state engineering of a hubbard system with ultracold fermions, *Physical review letters* **120**, 243201 (2018).
- [44] A. Kale, J. H. Huhn, M. Xu, L. H. Kendrick, M. Lebrat, C. Chiu, G. Ji, F. Grusdt, A. Bohrdt, and M. Greiner, Schrieffer-wolff transformations for experiments: Dynamically suppressing virtual doublon-hole excitations in a fermi-hubbard simulator, *Physical Review A* **106**, 012428 (2022).
- [45] G. Ji, M. Xu, L. H. Kendrick, C. S. Chiu, J. C. Brüggengjürgen, D. Greif, A. Bohrdt, F. Grusdt, E. Demler, M. Lebrat, *et al.*, Coupling a mobile hole to an antiferromagnetic spin background: Transient dynamics of a magnetic polaron, *Physical Review X* **11**, 021022 (2021).
- [46] C. S. Chiu, G. Ji, A. Bohrdt, M. Xu, M. Knap, E. Demler, F. Grusdt, M. Greiner, and D. Greif, String patterns in the doped hubbard model, *Science* **365**, 251 (2019).
- [47] M. F. Parsons, F. Huber, A. Mazurenko, C. S. Chiu, W. Setiawan, K. Wooley-Brown, S. Blatt, and M. Greiner, Site-resolved imaging of fermionic li 6 in an optical lattice, *Physical review letters* **114**, 213002 (2015).
- [48] J. Simon, W. S. Bakr, R. Ma, M. E. Tai, P. M. Preiss, and M. Greiner, Quantum simulation of antiferromagnetic spin chains in an optical lattice, *Nature* **472**, 307 (2011).
- [49] M. Greiner, C. Regal, C. Ticknor, J. Bohn, and D. Jin, Detection of spatial correlations in an ultracold gas of fermions, *Physical review letters* **92**, 150405 (2004).
- [50] L. W. Cheuk, M. A. Nichols, M. Okan, T. Gersdorf, V. V. Ramasesh, W. S. Bakr, T. Lompe, and M. W. Zwierlein, Quantum-gas microscope for fermionic atoms, *Physical review letters* **114**, 193001 (2015).
- [51] A. Sommer, M. Ku, G. Roati, and M. W. Zwierlein, Universal spin transport in a strongly interacting fermi gas, *Nature* **472**, 201 (2011).
- [52] M. Zwierlein, C. Schunck, C. Stan, S. Raupach, and W. Ketterle, Formation dynamics of a fermion pair condensate, *Physical review letters* **94**, 180401 (2005).
- [53] J. Hertkorn, J.-N. Schmidt, F. Böttcher, M. Guo, M. Schmidt, K. Ng, S. Graham, H. Büchler, T. Langen, M. Zwierlein, *et al.*, Density fluctuations across the superfluid-supersolid phase transition in a dipolar quantum gas, *Physical Review X* **11**, 011037 (2021).
- [54] T. Hartke, B. Oreg, C. Turnbaugh, N. Jia, and M. Zwierlein, Direct observation of nonlocal fermion pairing in an attractive fermi-hubbard gas, *Science* **381**, 82 (2023).
- [55] R. Blankenbecler, D. Scalapino, and R. Sugar, Monte carlo calculations of coupled boson-fermion systems. i, *Physical Review D* **24**, 2278 (1981).
- [56] S. R. White, D. J. Scalapino, R. L. Sugar, E. Loh, J. E. Gubernatis, and R. T. Scalettar, Numerical study of the two-dimensional hubbard model, *Physical Review B* **40**, 506 (1989).
- [57] J. E. Hirsch, Two-dimensional hubbard model: Numerical simulation study, *Physical Review B* **31**, 4403 (1985).
- [58] F. Werner, O. Parcollet, A. Georges, and S. Hassan, Interaction-induced adiabatic cooling and antiferromagnetism of cold fermions in optical lattices, *Physical review letters* **95**, 056401 (2005).
- [59] W. C. de Freitas Silva, M. V. Araujo, S. Roy, A. Samanta, N. d. C. Costa, N. Trivedi, and T. Paiva, Effects of strong electronic interactions on the thermopower properties of the repulsive hubbard model, *Physical Review B* **108**, 075101 (2023).
- [60] S. Roy, A. Samanta, and N. Trivedi, in preparation, .
- [61] A. J. Kim, F. Simkovic IV, and E. Kozik, Spin and charge correlations across the metal-to-insulator crossover in the half-filled 2d hubbard model, *Physical Review Letters* **124**, 117602 (2020).
- [62] A.-M. Daré, L. Raymond, G. Albinet, and A.-M. Tremblay, Interaction-induced adiabatic cooling for antiferromagnetism in optical lattices, *Physical Review B* **76**, 064402 (2007).
- [63] T. Paiva, R. Scalettar, M. Randeria, and N. Trivedi, Fermions in 2d optical lattices: temperature and entropy scales for observing antiferromagnetism and superfluidity, *Physical Review Letters* **104**, 066406 (2010).
- [64] C. Varney, C.-R. Lee, Z. Bai, S. Chiesa, M. Jarrell, and R. Scalettar, Quantum monte carlo study of the two-dimensional fermion hubbard model, *Physical Review B* **80**, 075116 (2009).
- [65] C. Sanner, E. J. Su, A. Keshet, R. Gommers, Y.-i. Shin, W. Huang, and W. Ketterle, Suppression of density fluctuations in a quantum degenerate fermi gas, *Physical re-*

- view letters **105**, 040402 (2010).
- [66] T. Müller, B. Zimmermann, J. Meineke, J.-P. Brantut, T. Esslinger, and H. Moritz, Local observation of antibunching in a trapped fermi gas, *Physical review letters* **105**, 040401 (2010).
- [67] C. Walsh, P. Sémon, G. Sordi, and A.-M. Tremblay, Critical opalescence across the doping-driven mott transition in optical lattices of ultracold atoms, *Physical Review B* **99**, 165151 (2019).
- [68] M. Endres, M. Cheneau, T. Fukuhara, C. Weitenberg, P. Schauß, C. Gross, L. Mazza, M. C. Bañuls, L. Pollet, I. Bloch, *et al.*, Single-site-and single-atom-resolved measurement of correlation functions, *Applied Physics B* **113**, 27 (2013).
- [69] P. Prelovšek, J. Kokalj, Z. Lenarčič, and R. H. McKenzie, Holon-doublon binding as the mechanism for the mott transition, *Physical Review B* **92**, 235155 (2015).
- [70] P. Phillips, Colloquium: Identifying the propagating charge modes in doped mott insulators, *Reviews of Modern Physics* **82**, 1719 (2010).
- [71] S. Zhou, Y. Wang, and Z. Wang, Doublon-holon binding, mott transition, and fractionalized antiferromagnet in the hubbard model, *Physical Review B* **89**, 195119 (2014).
- [72] T. Sato and H. Tsunetsugu, Dynamical characteristics of the mott transition: Examination of doublon dynamics in a triangular-lattice hubbard model, *Physics Procedia* **75**, 376 (2015).
- [73] T. Paiva, R. Scalettar, C. Huscroft, and A. McMa-
- han, Signatures of spin and charge energy scales in the local moment and specific heat of the half-filled two-dimensional hubbard model, *Physical Review B* **63**, 125116 (2001).
- [74] A. Macridin, M. Jarrell, T. Maier, P. Kent, and E. D’Azevedo, Pseudogap and antiferromagnetic correlations in the hubbard model, *Physical review letters* **97**, 036401 (2006).
- [75] B. Kyung, S. Kancharla, D. Sénéchal, A.-M. Tremblay, M. Civelli, and G. Kotliar, Pseudogap induced by short-range spin correlations in a doped mott insulator, *Physical Review B* **73**, 165114 (2006).
- [76] F. Boschini, M. Zonno, E. Razzoli, R. P. Day, M. Michiardi, B. Zwartsenberg, P. Nigge, M. Schneider, E. H. da Silva Neto, A. Erb, *et al.*, Emergence of pseudogap from short-range spin-correlations in electron-doped cuprates, *npj Quantum Materials* **5**, 6 (2020).
- [77] F. Krien, P. Worm, P. Chalupa-Gantner, A. Toschi, and K. Held, Explaining the pseudogap through damping and antidamping on the fermi surface by imaginary spin scattering, *Communications Physics* **5**, 336 (2022).
- [78] M. Vekić and S. White, Pseudogap formation in the half-filled hubbard model, *Physical Review B* **47**, 1160 (1993).
- [79] B.-B. Chen, C. Chen, Z. Chen, J. Cui, Y. Zhai, A. Weichselbaum, J. von Delft, Z. Y. Meng, and W. Li, Quantum many-body simulations of the two-dimensional fermi-hubbard model in ultracold optical lattices, *Physical Review B* **103**, L041107 (2021).